Extracellular Vesicle 6 (2025) 100094

Contents lists available at ScienceDirect

Extracellular Vesicle

journal homepage: www.elsevier.com/locate/vesic

Encapsulating extracellular vesicles with a minimal RISC complex as novel gene silencing tool

Tao Qiu *, Yu Yan, Rui Hu, Yuan Yi, Guowu Liu, Wenqiang Lu, Xin Zhou, Ke Xu **

Vesicure Therapeutics, Biobay 3B, Suzhou Industrial Park, Suzhou, China

ARTICLE INFO

Keywords:
Extracellular vesicles engineering
Gene silencing
Macrophage polarization

ABSTRACT

Gene silencing modalities including small interfering RNAs (siRNAs) and antisense oligonucleotides (ASOs) have prospered in both fundamental research and clinical translations in recent years, with delivery platform being one of the key elements for success. Extracellular vesicles (EVs) as natural carriers for cell-cell communication have been engineered in a variety of ways as delivery platform for gene silencing, yet facing limited efficiency and reproducibility. In this study, we developed a new strategy for engineering EVs as gene silencing tool. A minimal RNA-induced silencing complex (RISC), composing of modified Argonaute 2 (AGO2) protein and specially designed guide strand RNAs, were encapsulated into EVs and elicited prominent EGFP silencing in proof-of-concept study. This modular EVs platform, which we named as minRISC-EVs, efficiently silenced iNOS expression in M1 macrophages as well as STAT6/A20 expression in M2 macrophages, enabling macrophages polarization towards desired directions. The macrophage modulating ability was further validated *in vivo*, as minRISC-EVs against iNOS alleviated mice lung inflammation in lipopolysaccharide (LPS)-induced acute lung injury model, and minRISC-EVs against STAT6/A20 inhibited B16F10 tumor progression in the tumor xenograft model. In summary, minRISC-EVs can be utilized as novel gene silencing tool, and hold great promise for clinical translation in the future.

1. Introduction

Gene silencing technologies have revolutionized both fundamental biological research and therapeutic development, by enabling precise modulation of gene expression.[1] The current landscape of gene silencing technologies encompasses several established approaches, including siRNAs and ASOs, each with its own set of advantages and limitations.[2,3] A common challenge hindering the application of these tools remains in delivery. Current delivery systems, such as synthetic nanoparticles and various forms of conjugates, face limitations including immunogenicity, off-target effects, and unfavored biodistribution.[4]

In recent years, extracellular vesicles (EVs) have attracted significant attention as naturally derived, biocompatible carriers for various therapeutic cargoes.[5,6] Derived from multiple cellular origins, EVs comprise subtypes such as exosomes and microvesicles and possess a lipid bilayer that facilitates the encapsulation and protection of nucleic acids, proteins, and lipids from degradation.[7] Their intrinsic properties—including low immunogenicity, ability to cross physiological barriers, and innate targeting capabilities—present distinct advantages over traditional viral and non-viral delivery systems.[5,6]

Despite their potential, the application of EVs for gene silencing has been hindered by technical challenges. Previous engineering strategies mostly fell into the following two categories: (1) Exogenous loading methods. Chemically synthesized siRNAs or ASOs were loaded into purified EVs through direct incubation, electroporation or chemical reagent-based transfection.[8,9] (2) Endogenous loading methods. Donor cells were genetically engineered to overexpress siRNAs or miRNAs, such that the secreted EVs were naturally enriched with functional small RNAs.[8,9] Since exogenous loading methods rely on chemically synthesized materials, adding to the cost besides EVs production and purification, we prefer endogenous loading methods to acquire EVs with cargoes ready. Therefore, we set to develop a novel, robust EVs platform as gene silencing tool.

* Corresponding author.
** Corresponding author.
E-mail addresses: tao.qiu@vesicure.com (T. Qiu), ke.xu@vesicure.com (K. Xu).

https://doi.org/10.1016/j.vesic.2025.100094
Received 20 May 2025; Received in revised form 28 August 2025; Accepted 8 September 2025
Available online 16 September 2025

2. Materials and methods

2.1. Cell culture and transfection

Suspension-adapted HEK293 cell line (A23109, Quacell) was cultured in OPM-CD05 medium (81075-001, OPM Biosciences) and maintained on orbital shaker at 90 RPM in a humidified incubator at 37 °C with 8 % CO2. RAW264.7 (CL-0190, Procell) and B16F10 (CL-0319, Procell) were cultured in DMEM medium (11965092, Gibco) supplemented with 10 % FBS (A5669701, Gibco) and maintained in a humidified incubator at 37 °C with 5 % CO_2. Cells were passaged every 2–3 days.

For transfection of HEK293 cells, the cells were seeded to density around 2.5E+6 cells/mL. Plasmids were transfected with Transporter 5 transfection reagent (26008, Polysciences) at 1 μg plasmid/4 μg PEI ratio per 1 mL cell culture. The cells were harvested at 72 h post transfection.

2.2. EVs isolation from cell culture medium

The cell culture supernatant was first filtered through 0.45 μm filter units (SLHPR33RB, Millipore), followed by centrifugation (SW32Ti, Beckman Coulter) at 133,900 g at 4 °C for 60 min. The crude EVs pellet were washed once in PBS, and centrifuged again at 133,900 g at 4 °C for 60 min. The refined EVs were finally resuspended in PBS (10010, Gibco), and stored in −80 °C freezer.

2.3. Western blot analysis

The cells or EVs samples were first lysed with RIPA lysis buffer (R0010, Solarbio) on ice for 20 min. Then the total protein were quantified with MicroBCA protein assay kit (23235, Thermo scientific). After that, SDS-PAGE protein loading buffer (BL502A, Beyotime) was added into the samples and incubated at 95 °C for 10 min. Equal quantity of proteins for each sample was loaded onto 4–12 % SurePAGE™, Bis-Tris gels (M00653, GenScript). After electrophoresis (170 V, 35 min), the proteins were transferred onto PVDF membrane (ISEQ00010, Millipore). The membranes were blocked with QucikBlockTM Western blocking buffer (P0252, Beyotime) for 1h at room temperature (RT) before incubation with primary antibodies overnight at 4 °C. After extensive washing with TBST wash buffer (ST673, Beyotime), the membrane was further incubated for 2h at RT with HRP conjugated secondary antibodies. Following extensive washes with TBST buffer, the membranes were incubated with Pierce ECL Western Blotting Substrate (32209, Thermo scientific) and visualized with Tannon 5200 imager (Tannon).

The following antibodies were used: CD9 (abcam, AB263019) (1:1000), CD81 (Cell Signaling Technology, 56039S) (1:1000), Calnexin (abcam, ab22595) (1:1000), AGO2 (Cell Signaling Technology, 2897), VSVG (Santa Cruz, sc-365019), HRP Goat Anti-Rabbit IgG (H + L) (ABclonal, AS014), HRP Goat Anti-Mouse IgG (H + L) (ABclonal, AS003).

2.4. Transmission electron microscopy

EVs were applied onto the glow-discharged copper grid (200 mesh, coated with carbon film). To perform negative staining, 2 % uranyl acetate were incubated with EVs at room temperature for 1 min, followed by quick wash with distilled water to remove excess stain. The grids were air-dried before being imaged under Tecnai G2 transmission electron microscope (Thermo FEI, 120 kV).

2.5. Nanoparticle tracking analysis (NTA)

To evaluate the size distribution and concentration, EVs samples were freshly diluted at 1000–50,000 fold in 0.22-mm filtered PBS and analyzed immediately with ZetaView Nano Particle Tracking Analyzer (ParticleMetrix, PMX120-Z).

2.6. RT-qPCR

Total RNA from the cells plated on 96 well plates were first extracted and purified using the RNAprep Pure Micro Kit (DP420, TIANGEN). The concentration and quality of isolated RNA were detected using a NanoDrop (ThermoFisher). Reverse transcription was performed with HiScript Ill cDNA Synthesis Kit (R312-01, Vazyme). Next, the cDNA was added into the 2xSYBR green qPCR mix (A0012-R2, Ezbioscience), and quantitative PCR were analyzed with QuantStudio3 (Applied Biosystems).

2.7. Macrophage polarization assay

In polarization experiments, RAW264.7 cells were seeded at 20000 cells per well in 96-well flat-bottom tissue culture plates and cultured in polarizing medium overnight. M1 polarization of RAW264.7 cells was induced by 100 ng/mL Lipopolysaccharides (tlrl-3pelps, Invivogen) and 2.5 ng/mL IFN-γ (575302, Biolegend) for 24 h. M2 polarization of RAW264.7 cells was induced by 20 ng/mL IL-4 (574302, Biolegend) for 24 h.

2.8. EGFP silencing analysis

EGFP stably expressing HEK293 cell line was established in house. The cells were seeded at 30000 cells per well in 96-well flat-bottom tissue culture plates, before treated with 1E+10 total EVs particles. At 48 h post treatment, EGFP fluorescence was analyzed under fluorescent microscope (Thermo Fisher, EVOS 5000).

To quantitatively analyze EGFP silencing, the cells were harvested and resuspended in PBS for flow cytometric analysis. Cellular acquisition was performed using a BD FACS Celesta flow cytometer with a minimum threshold of 10,000 events per sample. Data analysis was conducted with FlowJo software (v7.6).

2.9. B16F10 tumor xenograft model

Female, 8 weeks old C57BL6/J mice (GemPharmat) were implanted with 1E6 B16F10 cells/mice under the right fat pad region. When the average tumor volume reached around 60 mm^3, the mice were randomly grouped for different treatment conditions. Intratumoral injections and tumor volume measurement were performed every day for seven days consecutively. On last day, mice were sacrificed and tumors were excised out and imaged.

2.10. LPS induced acute lung injury model

To establish acute lung injury model, 8 weeks old C57BL6/J mice (GemPharmat) were nasal instilled with 50 μL LPS (tlrl-eklps, InvivoGen) at 5 mg/kg dose. For EVs treatment, EVs were adminstrated by pulmonary nebulization using Micro Sprayer Aerosolizer (Y655650918, YuYanbio), at 50 μL volume in PBS per mouse. At the end of the experiment, mice were euthanized, and lung, serum and bronchoalveolar lavage fluid (BALF) samples were collected.

2.11. Cytokines analysis in BALF samples

The BALF supernatants were collected, centrifuged at 1000×*g* for 10 min at 4 °C, and cytokine levels were measured by mouse cytometric bead array (CBA) Kit (BD Biosciences). Briefly, 50 μL of samples (BALF supernatants) or known concentrations of standard samples (0–5000 pg/mL) were added to a mixture of 50 μL each of capture antibody bead reagent and phycoerythrin (PE)-conjugated detection antibody. The mixture was then incubated for 2 h at room temperature in the dark and

then washed to remove unbound detection antibody. Data were acquired using a FACSCelesta cytometer and analyzed using CBA software FACP V3.0.

2.12. Histological analysis

Tissue samples obtained from the C57BL6/J mice were first fixed in 4 % paraformaldehyde at 4 °C overnight, then dehydrated in 30 % (w/v) sucrose solution (A610498, Sangon Biotech) for 2 days. The dehydrated samples were then embedded in Tissue-Tek O.C.T Compound (4583, SAKURA) blocks and frozen overnight. Sections acquired at 5 μm thick sections were fixed at 4 % paraformaldehyde for 10 min before staining with hematoxylin and eosin (C0105M, Beyotime). Imaging analysis were performed under light microscope (MF43N, Mshot).

2.13. Transcriptome sequencing analysis

For mRNA sequencing, 1 μg total RNA was used for following library preparation. The poly(A) mRNA isolation was performed using Oligo (dT) beads. The mRNA fragmentation was performed using divalent cations and high temperature. Priming was performed using Random Primers. First strand cDNA and the second-strand cDNA were synthesized. The purified double-stranded cDNA was then treated to repair both ends and add a dA-tailing in one reaction, followed by a T-A ligation to add adaptors to both ends. Size selection of Adaptor-ligated DNA was then performed using DNA Clean Beads. Each sample was then amplified by PCR using P5 and P7 primers and the PCR products were validated. Then libraries with different indexs were multiplexed and loaded on an Illumina HiSeq/Illumina Novaseq/MGI2000 instrument for sequencing using a 2x150 paired-end (PE) configuration according to manufacturer's instructions.

For microRNA sequencing, 10 ng small RNA was used for library preparation. 3′SR Adaptor for Illumina was ligated to the small RNA using 3′Ligation Enzyme. To prevent adaptor-dimer, the excess of 3 ′SR Adaptor were hybrid with SR RT Primer for Illumina. 5′SR Adaptor for Illumina was ligated to the small RNA using 5′Ligation Enzyme and first strand cDNA was synthesized using ProtoScript II Reverse Transcriptase. Each sample was then amplified by PCR using P5 and P7 primers, the PCR products were purified by DNA clean beads. The purified products of 140-160bp were recovered and cleaned up using PAGE, validated using an Agilent 2100 Bioanalyzer. Then libraries with different indexes were multiplexed. The qualified libraries were sequenced pair end PE150 on the illumina HiseqXten/Novaseq/MGI2000 System.

2.14. AGO2 ELISA

To determine AGO2 concentration in EVs, the Sandwich ELISA kit (FineTest, EH6174) was used according to manufacturer's protocol. EVs were first permeabilized by incubating with lysis buffer (PBS+0.3 % TritonX-100) at room temperature for 30 min, before proceeding to ELISA quantification.

2.15. Statistical analysis

Experimental replicates were defined in the figure legends for each experiment. Statistical analyses were performed in GraphPad Prism 7 using student's t-test for experiments with two groups or one-way analysis of variance (ANOVA) for experiments with three or more groups. Values were expressed as mean ± standard deviation (SD) or as mean ± standard error of the mean (SEM), as indicated in the figure legends. Significance labeling and p values were presented in figures descriptions.

3. Results

3.1. Engineering EVs with a minimal RISC complex for gene silencing

The RNA-induced silencing complex (RISC) mediates endogenous RNAi pathway.[10] Mechanistically, a guide RNA is indispensable for finding the right target mRNA, and Argonaute 2 (AGO2) protein is critical for subsequent mRNA degradation or translational repression.[10] The presence of AGO2 in complex with small RNAs have been reported in naturally secreted, unmodified EVs, which demonstrated gene silencing activity at physiological-relevant level.[11,12] Several studies have tried to enrich the AGO2-RNA complex in EVs for higher gene silencing activity, for instance, to elevate AGO2 level in EVs by fusing AGO2 with EVs marker protein CD9,[13] or to increase small RNA level in EVs by overexpressing double strand RNAs in donor cells.[14] We noticed that those attempts were often focused on improving a particular element from this minimal RISC complex (minRISC), without optimizing the other factors. Thus, we decided to systematically optimize the engineering strategies for encapsulating a minimal RISC complex into EVs with high efficiency.

To generate guide RNA for the minimal RISC complex, short-hairpin RNA (shRNA) overexpression construct was designed to form the classical "22 + 7" structure: 22 nt sense-strand pairing with 22 nt antisense-strand, and 7 nt unpaired region forming the stem-loop (Fig. 1A). Next, to load AGO2 protein into EVs with high abundancy, the EVs scaffold protein BASP1 was used since it outperformed the majority of EVs marker proteins.[15] BASP1 was directly fused to the N-terminus of AGO2 through a flexible $(GGGGS)_3$ linker. The shRNA and AGO2 overexpression cassettes were integrated into one plasmid (minRISC plasmid) (Fig. 1A). Finally, to facilitate the endosomal escape of EVs cargo following recipient cells endocytosis, the fusogenic protein vesicular stomatitis virus G glycoprotein (VSVG) expression construct was also included to pseudotype the EVs membrane with VSVG protein (Fig. 1A).

To benchmark the silencing efficacy of this initial design, target sequences against EGFP were designed into the shRNA constructs for intuitive EGFP silencing. Suspension-adapted HEK293 cells cultured in serum-free medium were used as the EVs donor cells. Three groups were set up as follow: VSVG only group (EVs donor cells transfected with VSVG plasmid only), minRISC only group (EVs donor cells transfected with minRISC plasmid only) and VSVG + minRISC group (EVs donor cells transfected with both VSVG and minRISC plasmid). At 72 h post transfection, EVs were collected from the culture medium by ultracentrifugation. Nanoparticle tracking analysis (NTA) revealed that all three groups of EVs had similar size distribution, with peak diameter around 120 nm (Fig. 1B). Transmission electron micrography demonstrated that all three groups of EVs presented typical vesicular morphology (Fig. 1C). Western blot analysis showed VSVG and AGO2 protein enrichment in EVs as expected, and that EVs were positive for CD9, CD81 markers and negative for calnexin markers (Fig. 1D).

HEK293 cells stably expressing EGFP were used as recipient cells to test the silencing ability of EVs. Total 1E10 EVs particles were added to 3E4 cells seeded per well, and EGFP fluorescence were evaluated after 48 h. As shown in Fig. 1E, cells receiving EVs expressing both minRISC and VSVG had apparently dimer EGFP fluorescence under microscope, whereas VSVG-only and minRISC-only EVs did not affect EGFP fluorescence at all. Consistently, flow cytometry analysis revealed that EVs expressing both minRISC and VSVG resulted in around 50 % EGFP knock-down, in contrast to non-effect from VSVG-only and minRISC-only EVs (Fig. 1F–G). In summary, EVs engineered with minimal RISC complex and VSVG demonstrated considerable gene silencing ability, which we named as minRISC-EVs.

3.2. Optimization of guide RNA precursor design for minRISC-EVs

As the proof-of-concept design was successful, we set out to optimize

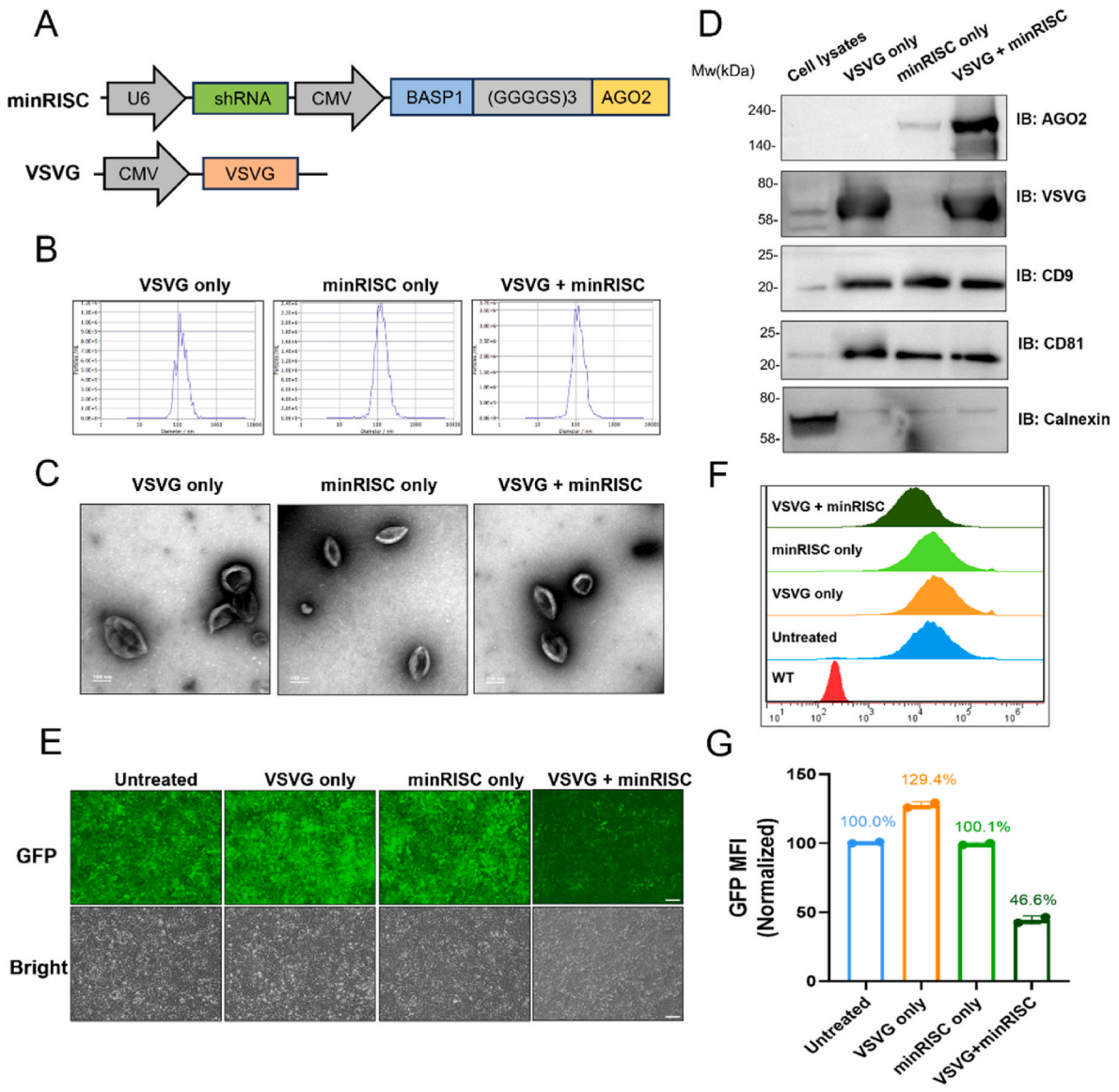

Fig. 1. Engineering EVs with a minimal RISC complex for gene silencing. (A) Schematic diagram showing the overexpression constructs design. (B) Nanoparticle tracking analysis for EVs overexpressing VSVG only, minRISC only and VSVG + minRISC. (C) Representative transmission electron micrographs of EVs from different groups. Scale bar: 100 nm. (D) Western blot analysis for cell lysates and EVs from different groups. (E) Fluorescent microscopy analysis for cells received EVs from different groups. Scale bar: 20 μm. (F) Flow cytometry analysis for cells received different groups of EVs. (G) Flow cytometry quantification presented as mean fluorescence intensity (MFI) normalized to untreated group; each data point represents at least 10,000 cells. N = 2. Values are plotted as mean ± SD.

the performance of minRISC-EVs. To begin with, various strategies had been proposed to enhance shRNA-mediated gene silencing efficiency. Shortening the stem length of shRNA below 20 nt results in alternative processing that bypasses Dicer, resulting in AGO2-specific shRNA (agshRNA) with higher silencing efficiency.[16] Another shRNA alternative named single-stranded, AGO2-processed interfering RNA (saiRNA), utilized a hepatitis delta virus (HDV) ribozyme sequence to generate a clean 3′ overhang at sense-strand, were also reported to improve silencing ability.[17] Therefore, shRNA, agshRNA and saiRNA were compared head-to-head in minRISC-EVs system. The agshRNA construct was designed as follow: 17 nt antisense-strand base pairing with 17 nt sense-strand, with additional 4 nt stem-loop sequences (Fig. 2A). The saiRNA fused HDV ribozyme sequence to the 3' of sense-strand on the agshRNA scaffold (Fig. 2A). To note, shRNA, agshRNA and saiRNA target sequences were designed for the same EGFP region, to allow unbiased comparison.

The minRISC-EVs assembled with either shRNA, agshRNA or saiRNA were acquired and showed similar expression level for AGO2 and VSVG protein (Fig. 2B). EGFP silencing efficiency evaluation by microscopy imaging showed that saiRNA had the best performance among all three RNA precursor designs, resulted in significantly dimer EGFP fluorescence when minRISC-EVs were added to recipient cells at equal number (1E10 particles per 3E4 cells) (Fig. 2C). Flow cytometry analysis further revealed that minRISC-EVs with saiRNA precursor led to overall 75 % EGFP knock-down compared to 60 % by agshRNA and 50 % by shRNA (Fig. 2D–E). Hence, saiRNA design was superior and was used for all subsequent optimization studies.

3.3. *The choice for linker peptides was insignificant for minRISC-EVs efficiency*

BASP1 is a peripheral membrane protein, anchored to the inner leaflet of membranes through N-terminus myristoylation modification.[15] Since RISC complex predominantly localize in the cytoplasmic mRNA decay centers known as P-bodies, we reasoned that a cleavable linker could relieve AGO2 from the spatial constraint by BASP1, thereby

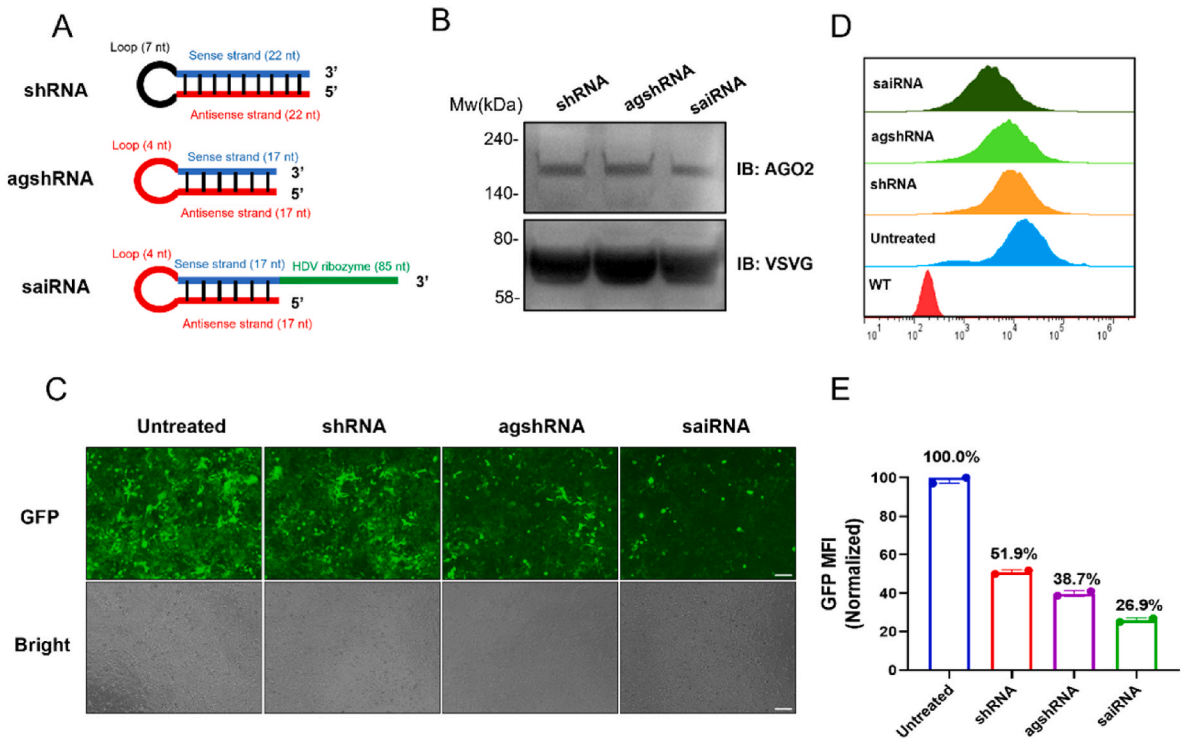

Fig. 2. Optimization of guide RNA precursor design for minRISC-EVs (A) Schematic diagram showing shRNA, agshRNA and saiRNA construct design for minRISC-EVs. (B) Western blot analysis for EVs from different groups. (C) Fluorescent microscopy analysis for cells received EVs from different groups. Scale bar: 20 μm. (D) Flow cytometry analysis for cells received EVs from different groups. (E) Flow cytometry quantification presented as mean fluorescence intensity (MFI) normalized to untreated group; each data point represents at least 10,000 cells. N = 2. Values are plotted as mean ± SD.

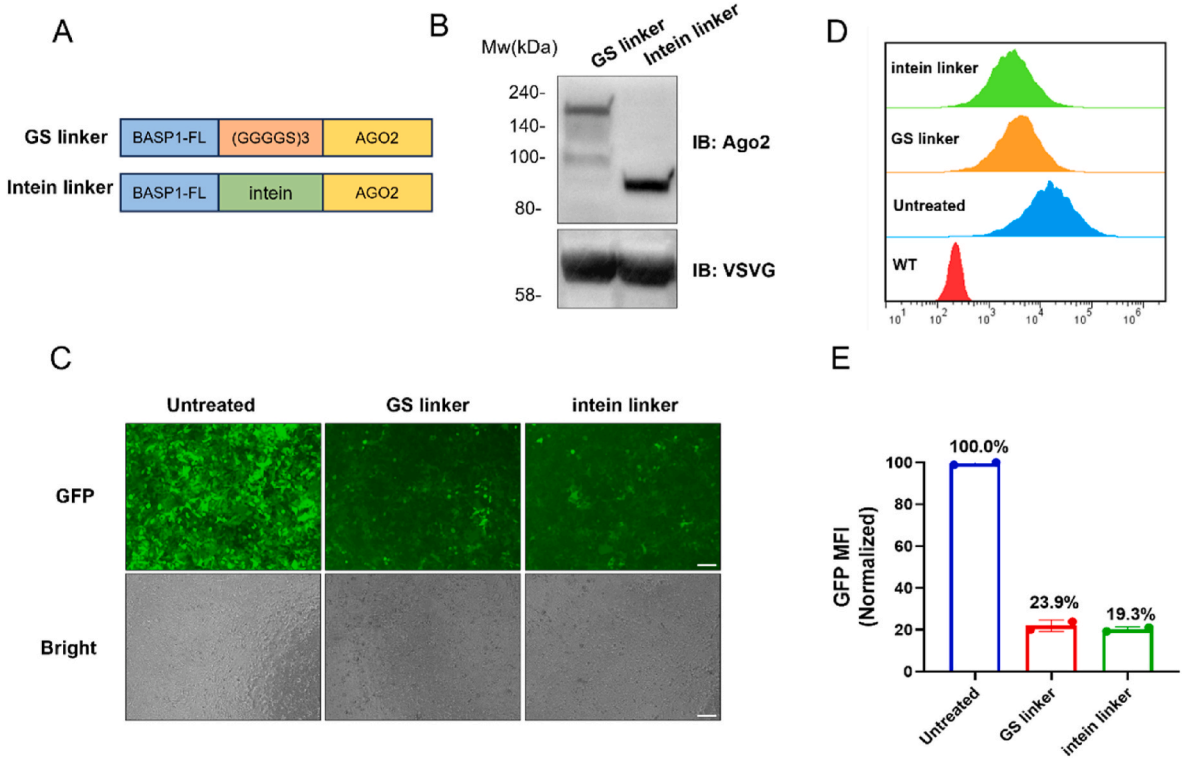

Fig. 3. The choice for linker peptides was insignificant for minRISC-EVs efficiency (A) Schematic diagram showing GS linker versus intein linker construct design for minRISC-EVs. (B) Western blot analysis for EVs from different groups. (C) Fluorescent microscopy analysis for cells received EVs from different groups. Scale bar: 20 μm. (D) Flow cytometry analysis for cells received EVs from different groups. (E) Flow cytometry quantification presented as mean fluorescence intensity (MFI) normalized to untreated group; each data point represents at least 10,000 cells. N = 2. Values are plotted as mean ± SD.

improving system efficiency further. The self-cleavable intein linker had been successfully used for EVs cargo loading, which enabled cargo release from EVs scaffold proteins.[18] Therefore, we set out to determine if intein linker would outperform GS linker in minRISC-EVs system (Fig. 3A). Western blot analysis for harvested EVs revealed AGO2 protein band around 90 kDa for intein linker design, in contrast to ~140 kDa band for GS linker design, indicating successful AGO2 release from BASP1(Fig. 3B). Interestingly, EGFP silencing evaluation showed that intein linker only had marginal improvement, with overall silencing rate close to that of GS linker (Fig. 3C–E). It appeared that conformational constraint of BASP1-AGO2 was not determinative factor in system efficiency. As the length of GS linker (15aa) was much shorter that intein linker (160aa), we decided to keep GS linker for subsequent studies.

3.4. Optimization of BASP1 length for enriching AGO2 in minRISC-EVs

Finally, we investigated if EVs scaffold protein could be improved. BASP1 associates with the inner leaflet of cellular membranes through N-terminal myristoylation as well as a polybasic effector domain.[15] Previous studies have shown that a minimal peptide from the N-terminus of BASP1 were sufficient for robust EVs cargo loading.[15] Therefore, we compared the performance of the first 10 residues from BASP1 (BASP1-N10, MGGKLSKKKK) versus BASP1 full length protein (BASP1-FL) in minRISC-EVs (Fig. 4A). BASP1-N10 loaded significantly higher amount of AGO2 protein into EVs (Fig. 4B). Correspondingly, BASP1-N10 version of minRISC-EVs resulted in robust EGFP silencing effect, reaching around 95 % EGFP silencing rate compared to 75 % by BASP1-FL (Fig. 4C–E). Therefore, BASP1-N10 as the EVs scaffold further improved the system efficiency.

3.5. Investigation of various fusogens in mediating minRISC-EVs silencing efficacy

The viral fusogen VSVG was indispensable for functions of minRISC-EVs, yet it faced limitations for *in vivo* applications, such as VSVG could be inactivated by human serum proteins, and that undesired humoral immunity could be induced upon VSVG administration.[19–21] To address this limitation, we set out to test a VSVG mutant (T230N/T368A) which has been reported to resist serum inactivation.[22] As demonstrated in Supplementary Fig. 1A–B, this serum-resistant VSVG mutant (T230N/T368A) had equivalent efficiency to VSVG wild type in mediating minRISC-EVs silencing effect. Therefore, at least part of VSVG's limitation can be solved by this mutant form.

Since various fusogens other than VSVG have been tested for improved functionality on lentiviral vectors and virus-like particles (VLPs), we are curious to see if substituting VSVG with these fusogens would benefit minRISC-EVs as well. Several reported fusogens were tested to replace VSVG in minRISC-EVs, including Syncytin,[23] GP64,[24] P14 and P15,[25] Myomixer and Myomaker.[26] As shown in Supplementary Fig. 1C–D, none of these fusogens could replace VSVG in mediating minRISC-EVs' function. We noticed that others have also tested various fusogens to pseudotype EVs to facilitate cargo release, and found that VSVG was the only fusogen that worked.[27] In conclusion, currently VSVG is the only choice for minRISC-EVs.

In summary, the optimized minRISC-EVs include the following components: (1) saiRNA as the precursor to generate guide RNAs (2) BASP1-N10 fused to AGO2 protein through GS linker, to load the minimal RISC complex into EVs (3) fusogen protein VSVG for enhanced endosome escape.

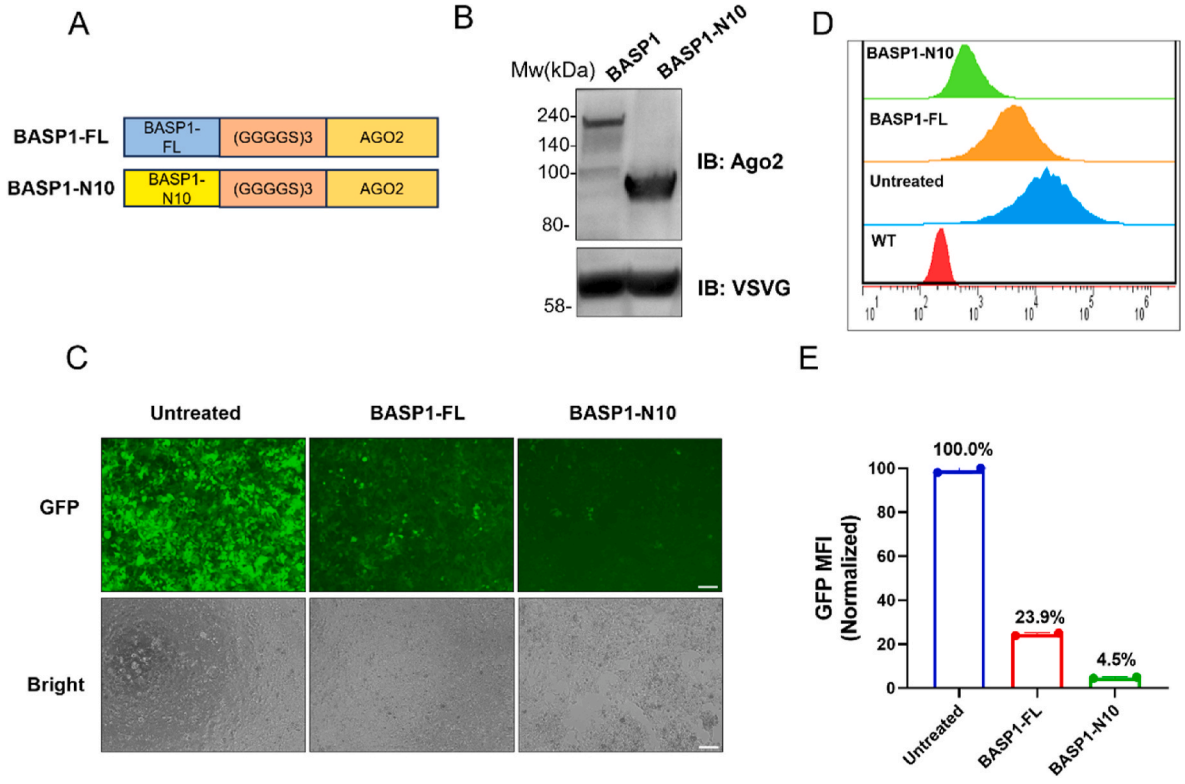

Fig. 4. Optimization of BASP1 length for enriching AGO2 in minRISC-EVs (A) Schematic diagram showing BASP1 full length versus BASP1-N10 construct design for minRISC-EVs. (B) Western blot analysis for EVs from different groups. (C) Fluorescent microscopy analysis for cells received EVs from different groups. Scale bar: 20 μm. (D) Flow cytometry analysis for cells received EVs from different groups. (E) Flow cytometry quantification presented as mean fluorescence intensity (MFI) normalized to untreated group; each data point represents at least 10,000 cells. N = 2. Values are plotted as mean ± SD.

3.6. Time course analysis for minRISC-EVs silencing efficacy in vitro

The optimization process for minRISC-EVs focused on evaluating silencing effect in short term (48 h). To investigate at a longer time scale, time course analysis was performed. A single dose of minRISC-EVs targeting EGFP were added to the EGFP-expressing HEK293 cells, and the EGFP silencing effect were evaluated for six consecutive days. As shown in Supplementary Fig. 2, the silencing efficacy by minRISC-EVs was highest at day 2 to day 3 post treatment, reaching around 80 % knock-down rate. At day 4 to day 6, the knock-down rate was gradually decreasing, quantified at 52 %, 39 % and 24 % respectively. Therefore, minRISC-EVs possess relatively short-term silencing ability (4 days in maximum).

3.7. Quantification of AGO2 protein level in minRISC-EVs

The dosage information of minRISC-EVs mainly relied on particles number as quantified by NTA analysis. To explicitly know how many cargoes were getting actively loaded into minRISC-EVs, ELISA analysis was performed to quantify AGO2 protein. Wild type EVs from non-engineered cells as well as minRISC-EVs were equally adjusted to 1E+12 particles/mL, before membrane permeabilization and AGO2 quantification. Interestingly, wild type EVs only contained low concentration of AGO2 proteins at 2.5 ng/mL, whereas minRISC-EVs enriched significantly higher amount of AGO2 at 250 ng/mL (Supplementary Fig. 3A–B). As converted to molecular numbers, each wild type EVs particle contained in average 0.015 AGO2 molecule, in contrast to 1.5 AGO2 molecule per minRISC-EV (Supplementary Fig. 3C). The engineering strategy effectively led to 100-fold enrichment for AGO2 protein cargo.

3.8. Global transcriptome analysis for minimal RISC complex EVs recipient cells

Although minRISC-EVs potently silenced EGFP expression, it was unknown whether significant off-target effect was present. Therefore, we performed transcriptome analysis for EGFP expressing HEK293 cells post minRISC-EVs silencing, to reveal gene expression changes globally. To begin with, mRNA sequencing was performed for untreated cells versus EGFP-silenced cells (Supplement Fig. 4A). Triplicate samples were set up for each group, and the significance threshold was determined as at least two-fold differential expression with adjusted p-value less than 0.05. Among around 250,000 total mRNA transcripts, 55 genes were significantly up-regulated and 55 genes were significantly down-regulated following minRISC-EVs treatment (Supplement Fig. 4B). Top-10 differential expressed genes were presented in heat map, and EGFP was the top-6 most down-regulated with around 75 % knock-down (Supplement Fig. 4C). None of essential house-keeping genes were found to be significantly affected.

Next, microRNA sequencing was performed for untreated cells versus EGFP-silenced cells (Supplement Fig. 4D). Triplicate samples were set up for each group, and the significance threshold was determined as at least two-fold differential expression with adjusted p-value less than 0.05. Among around 3000 total microRNA transcripts, 22 were significantly up-regulated and 14 were significantly down-regulated following minRISC-EVs treatment (Supplement Fig. 4E). Top-10 differential expressed transcripts were presented in heat map (Supplement Fig. 4F). Notably, the EGFP antisense strand was top-1 up-regulated sequences, quantified with more than 32,000-fold elevation, whereas the EGFP sense strand was not found at all in recipient cells. This result indicated that the saiRNA design worked as expected, in which minRISC-EVs delivered the target RNA strand but not the passenger strand to recipient cells with high efficiency.

Based on the high-throughput sequencing results, minRISC-EVs had minimal off-target effect in recipient cells' mRNA and microRNA transcriptome. One of the key reasons could be the lack of passenger strand in minRISC-EVs during biogenesis, thus eliminating the off-target effect in recipient cells deriving from passenger strand.

3.9. minRISC-EVs efficiently silenced STAT6 and A20 in M2 macrophage in vitro, and inhibited B16F10 tumor progression in xenograft model

To test if minRISC-EVs could efficiently silence target genes other than EGFP, we selected macrophage polarization genes for validation. The alternatively activated macrophages (M2 macrophages) are associated with anti-inflammatory reactions and tissue remodeling.[28] The signal transducer and activator of transcription 6 (STAT6) drives the M2 phenotype of macrophages.[29,30] Additionally, A20, also called tumor necrosis factor alpha induced protein 3 (TNFAIP3), is an endogenous negative regulator of NF-κB signaling, which has also been reported to drive the M2 polarization of macrophages.[31] Here, we selected both STAT6 and A20 as targets in M2 macrophages.

RAW264.7 cells were first polarized towards M2 phenotype by induction with interleukin-4 (IL-4), followed by treatment with minRISC-EVs targeting STAT6 or A20 for 48 h (Fig. 5A). Dose-dependent knock-down of both STAT6 and A20 were observed, with maximal knock-down efficiency over 80 % at highest dose (1.2E10 particles per 3E4 cells) (Fig. 5B). In contrast, the minRISC-EVs loaded with scramble sequences did not result any target genes knock-down (Fig. 5B). Correspondingly, 3- to 7-fold up-regulation of pro-inflammatory cytokines such as IL-1β, IL-6 and IL-12 were observed, indicating efficient pro-inflammatory conversion of M2 macrophages post minRISC-EVs treatment (Fig. 5C).

Since minRISC-EVs successfully modulated M2 macrophage driver gene expression and elevated the pro-inflammatory phenotypes *in vitro*, we set out to test if similar effect could be retained *in vivo*. B16F10 melanoma xenograft model was established in C57BL6/J mice. The minRISC-EVs against STAT6 and A20 were combined at 5E10 particles each, for intratumor injection for seven days consecutively (Fig. 5D). Immune checkpoint inhibitors PD1 antibody was included as monotherapy, as well as in combination therapy with minRISC-EVs to see if a synergistic effect could be produced. B16F10 tumor expanded rapidly in PBS treated groups as well as minRISC-Scramble treated groups, whereas minRISC-STAT6/A20 administration significantly inhibited tumor growth as measured by tumor size and tumor mass (Fig. 5E–F). Notably, minRISC-EVs monotherapy resulted in similar tumor inhibiton efficacy to PD1 monotherapy (Fig. 5E–F). However, the combination of minRISC-EVs and PD1 antibody did not lead to greater inhibitory effect, as similar tumor mass/weight were observed in comparison to either monotherapy (Fig. 5E–F). In summary, minRISC-EVs showed consistent efficacy in animal models as well.

3.10. minRISC-EVs efficiently silenced iNOS in M1 macrophage in vitro, and alleviated LPS-induced acute lung inflammation model

At the other direction of macrophage polarization, classically activated macrophages (M1 macrophages) are pro-inflammatory and have a central role in host defense against infection.[28] Inducible nitric oxide synthase (iNOS) expression served as a hallmark of M1 macrophages, contributing to the pro-inflammatory phenotype, making it a promising therapeutic target in inflammatory diseases. Therefore, to validate the effect of minRISC-EVs against iNOS on M1 macrophages, RAW264.7 cells were first polarized towards M1 phenotype by induction with lipopolysaccharide (LPS) and interferon-γ (IFN-γ). Next, minRISC-EVs against iNOS were added to those M1 cells (1.2E10 particles per 3E4 cells), followed by qPCR analysis for gene expression changes at 48 h post treatment (Fig. 6A). Around 60 % silencing efficiency was observed for minRISC-iNOS EVs, in contrast to the no effect from minRISC-EVs loaded with scramble sequences (Fig. 6B). At the phenotype level, iNOS knock-down by minRISC-EVs efficiently decreased the expression of pro-inflammatory cytokines including IL-1β, IL-6 and IL-12, indicating successful anti-inflammatory modulating effect as expected (Fig. 6C).

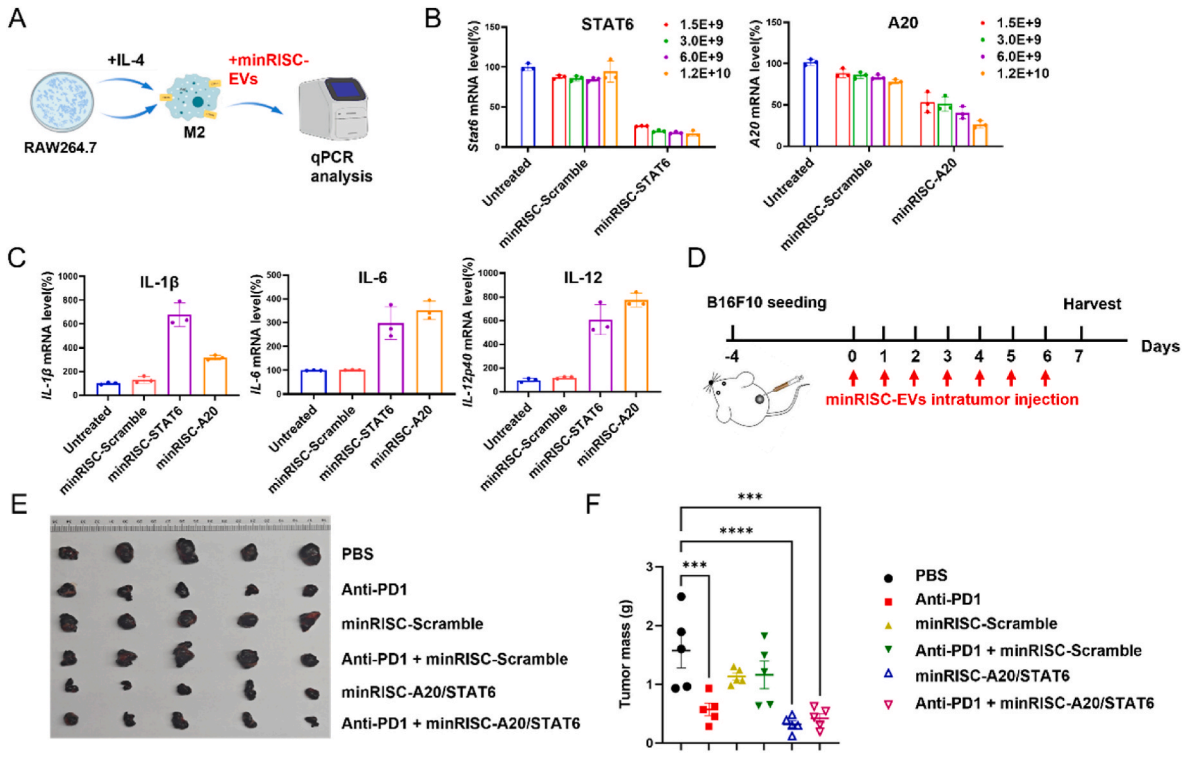

Fig. 5. minRISC-EVs efficiently silenced STAT6 and A20 in M2 macrophage *in vitro*, and inhibited B16F10 tumor progression in xenograft model (A) Schematic diagram showing RAW264.7 macrophages were first polarized towards M2 phenotype with IL-4, followed by minRISC-EVs treatment for 48 h. (B) QPCR analysis for STAT6 and A20 mRNA changes in minRISC-EVs treated M2 cells. EVs doses ranged from 1.5E+9 total particles to 1.2E+10 total particles. N = 3. (C) QPCR analysis for IL-1β, IL-6 and IL-12 mRNA changes in different groups. N = 3. (D) Schematics of B16F10 xenograft model in C57BL/6J mice. B16F10 cells were first implanted subcutaneously and grew to appropriate size, followed by minRISC-EVs intratumorally injection for 7 consecutive days. Mice were euthanized at day 7 for analysis. (E) Images of tumor at end point for different treatment groups.N = 5 (F) Tumor mass measurement at end point for different treatment groups. N = 5. ***: $p < 0.001$. ****: p value < 0.0001.

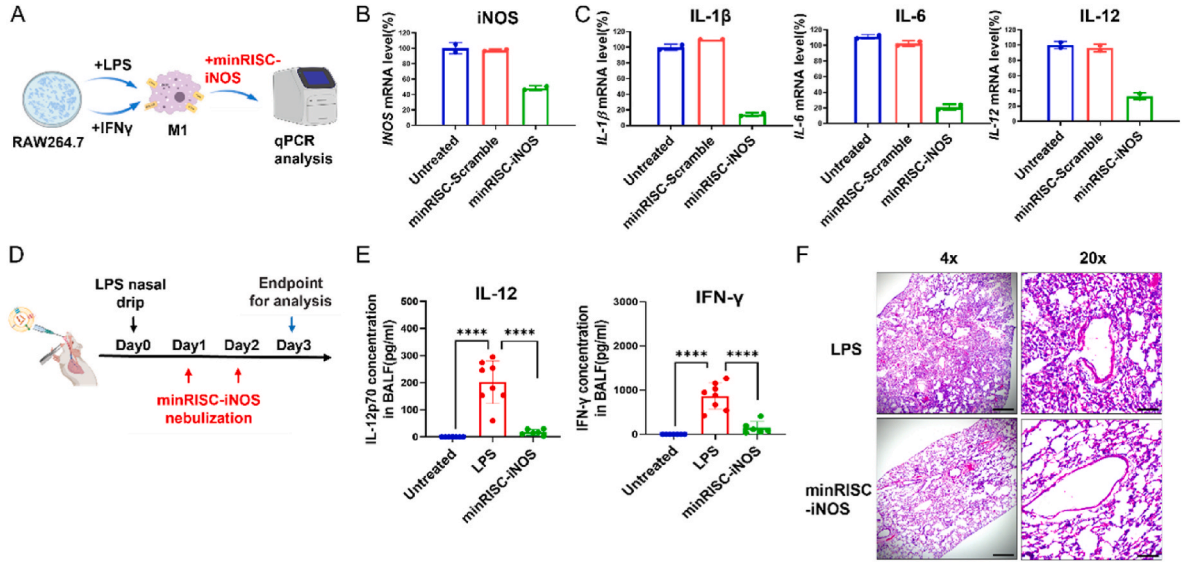

Fig. 6. minRISC-EVs efficiently silenced iNOS in M1 macrophage *in vitro*, and alleviated LPS-induced acute lung inflammation model (A) Schematic diagram showing RAW264.7 macrophages were first polarized towards M1 phenotype with LPS and IFN-γ, followed by minRISC-EVs treatment for 48 h. (B) QPCR analysis for iNOS mRNA changes in minRISC-EVs treated M1 cells. N = 3. (C) QPCR analysis for IL-1β, IL-6 and IL-12 mRNA changes in different groups. N = 3. (D) Schematics of acute lung injury model in C57BL/6J mice. A single dose of LPS nasal drip was administrated at day 0, followed by minRISC-EVs (against iNOS) administration for two consecutive days by nebulization. Mice were euthanized at day 3 for analysis. (E) Pro-inflammatory cytokines analysis in BALF from different groups. N = 8. ****: p value < 0.0001. (F) H&E analysis for lung sections from different groups. Scale bar: 500 μm (4x); 100 μm (20x).

Next, acute lung injury model was established in C57BL/6J mice by a single dose of LPS nasal drip, to evaluate if minRISC-EVs against iNOS treatment could alleviate lung inflammation (Fig. 6D). Following EVs administration by nebulization for two consecutive days (5E10 particles per dose), bronchoalveolar lavage fluid (BALF) were collected and analyzed for inflammatory cytokines level. As shown in Fig. 6E, LPS treatment induced high level of IL-12 and IFN-γ in BALF, whereas minRISC-EVs treatment significantly reduced these cytokines level. Hematoxylin and eosin (H&E) staining for lung sections revealed that LPS resulted in apparent interstitial and alveolar edema, as well as massive recruitment of lymphocytes into peribronchial, perivascular, and alveolar regions, whereas minRISC-EVs treatment significantly alleviated these histopathological changes (Fig. 6F). Therefore, minRISC-EVs targeting iNOS demonstrated potent anti-inflammatory effect *in vivo* as well.

4. Discussion

Multiple strategies have been developed to engineer EVs as gene silencing tools, yet generally facing limited efficacy and reproducibility.[32,32–34] Here we performed systemic optimization for encapsulating a minimal RISC complex into EVs, considering the guide RNA precursor design, AGO2 enrichment strategy, effect of distinct peptide linkers and the incorporation of membrane fusogen VSVG, which eventually led to robust gene silencing effect by the engineered EVs named as minRISC-EVs. We believe minRISC-EVs can serve as benchmark for utilizing EVs as gene silencing tool.

Target genes modulating either M1 or M2 macrophage phenotypes were chosen for minRISC-EVs validation in this study. The tumor-associated macrophages (TAMs) represent a critical target cell population for cancer therapy, and STAT6 is one of the key drivers for the immunosuppressive M2 phenotype.[29,30,35] Exosome-mediated delivery of nucleic acids targeting STAT6 had proved efficacy in tumor growth inhibition in mice models [36–42], and had also entered Phase 1 clinical trial for evaluation (NCT05375604). Here minRISC-EVs provide alternative method for STAT6 silencing without the need for chemically synthesized nucleic acids, which is highly advantageous in terms of cost. On the other hand, dysregulated iNOS has been implicated in numerous pathologies with no approved therapeutics to this date.[37] While small molecule is the main modality of iNOS inhibitors being developed, we here provide an RNA silencing approach with EVs as carrier, which could potentially overcome bottlenecks faced from other modalities.

Although minRISC-EVs demonstrated great potential in both cellular assays and animal models, a few limitations remained to be addressed. To start with, currently minRISC-EVs only possess short-term silencing ability (4 days in maximum). The long-term effect is absolutely the key for success in current gene silencing therapy, which is hypothesized to be attributed to several factors. Critically, majority of siRNA drugs are chemically modification on backbone, which help resist the degradation in lysosomes upon endocytosis.[38] Therefore, lysosomes can serve as depot to allow slow and steady releasing of siRNA drugs. Although minRISC-EVs' strength is the bio-generated guide RNAs with bio-generated delivery platform in ready form, it had to suffer from the short-term efficacy due to lack of chemistry modification. Next, the exact concentration of guide RNAs in minRISC-EVs were not quantified in this study. This information will be essential in determining the dosage effect for further studies. Since the AGO2 protein was quantified to 1.5 copy per minRISC-EV, it could be estimated that 1.2 nM guide RNAs were present in minRISC-EVs at 1E12 particle/mL, provided that 50 % AGO2 molecules were loaded with guide RNAs. Nonetheless, more accurate quantification method should be developed to determine the exact number.

For broadening the applicability of minRISC-EVs, several directions hold great promises. Currently, simultaneous multigene silencing by minRISC-EVs can only be achieved by combining multiple EVs preparations. This may be improved by integrating multiple precursor RNAs into one overexpression plasmid, such that a single preparation of minRISC-EVs could have multiple target RNAs ready. Furthermore, combining this minRISC-EVs framework with other EVs engineering strategies, for instance loading of additional small molecules for broader function,[8,9] or loading of surface targeting moiety for delivery to specific cell types,[39] could substantially improve the applicability of minRISCs-EVs for both fundamental research and clinical translations in future.

CRediT authorship contribution statement

Tao Qiu: Writing – original draft, Visualization, Investigation, Data curation, Conceptualization. **Yu Yan:** Investigation. **Rui Hu:** Investigation. **Yuan Yi:** Investigation. **Guowu Liu:** Investigation. **Wenqiang Lu:** Investigation. **Xin Zhou:** Investigation. **Ke Xu:** Writing – review & editing, Supervision, Conceptualization.

Declaration of competing interest

The authors declare that they have no known competing financial interests or personal relationships that could have appeared to influence the work reported in this paper.

Acknowledgments

Some illustrative graphics were created with biogdp.com. This study was funded by Vesicure Therapeutics.

Appendix A. Supplementary data

Supplementary data to this article can be found online at https://doi.org/10.1016/j.vesic.2025.100094.

References

1. Rajam MV. RNA silencing technology: a boon for crop improvement. *J Biosci*. 2020;45.
2. Collotta D, Bertocchi I, Chiapello E, Collino M. Antisense oligonucleotides: a novel Frontier in pharmacological strategy. *Front Pharmacol*. 2023;14, 1304342. https://doi.org/10.3389/fphar.2023.1304342.
3. Hu B, Zhong L, Weng Y, et al. Therapeutic siRNA: state of the art. *Signal Transduct Targeted Ther*. 2020;5(1):101. https://doi.org/10.1038/s41392-020-0207-x.
4. Paunovska K, Loughrey D, Dahlman JE. Drug delivery systems for RNA therapeutics. *Nat Rev Genet*. 2022;23(5):265–280. https://doi.org/10.1038/s41576-021-00439-4.
5. Du S, Guan Y, Xie A, et al. Extracellular vesicles: a rising star for therapeutics and drug delivery. *J Nanobiotechnol*. 2023;21(1):231. https://doi.org/10.1186/s12951-023-01973-5.
6. Kumar MA, Baba SK, Sadida HQ, et al. Extracellular vesicles as tools and targets in therapy for diseases. *Signal Transduct Targeted Ther*. 2024;9(1):27. https://doi.org/10.1038/s41392-024-01735-1.
7. van Niel G, D'Angelo G, Raposo G. Shedding light on the cell biology of extracellular vesicles. *Nat Rev Mol Cell Biol*. 2018;19(4):213–228. https://doi.org/10.1038/nrm.2017.125.
8. Ma Y, Dong S, Grippin AJ, et al. Engineering therapeutical extracellular vesicles for clinical translation. *Trends Biotechnol*. 2025;43(1):61–82. https://doi.org/10.1016/j.tibtech.2024.08.007.
9. Yang C, Xue Y, Duan Y, Mao C, Wan M. Extracellular vesicles and their engineering strategies, delivery systems, and biomedical applications. *J Contr Release*. 2024;365:1089–1123. https://doi.org/10.1016/j.jconrel.2023.11.057.
10. Hammond SM. Dicing and slicing: the core machinery of the RNA interference pathway. *FEBS Lett*. 2005;579(26):5822–5829. https://doi.org/10.1016/j.febslet.2005.08.079.
11. Lv Z, Wei Y, Wang D, Zhang CY, Zen K, Li L. Argonaute 2 in cell-secreted microvesicles guides the function of secreted miRNAs in recipient cells. *PLoS One*. 2014;9(7), e103599. https://doi.org/10.1371/journal.pone.0103599.
12. McKenzie AJ, Hoshino D, Hong NH, et al. KRAS-MEK signaling controls Ago2 sorting into exosomes. *Cell Rep*. 2016;15(5):978–987. https://doi.org/10.1016/j.celrep.2016.03.085.
13. Es-Haghi M, Neustroeva O, Chowdhury I, et al. Construction of fusion protein for enhanced small RNA loading to extracellular vesicles. *Genes*. 2023;14(2). https://doi.org/10.3390/genes14020261.
14. Wang C, Sheng W, Zhou Y, et al. siRNA-AGO2 complex inhibits bacterial gene translation: a promising therapeutic strategy for superbug infection. *Cell Rep Med*. 2025;6(3), 101997. https://doi.org/10.1016/j.xcrm.2025.101997.

15. Dooley K, McConnell RE, Xu K, et al. A versatile platform for generating engineered extracellular vesicles with defined therapeutic properties. *Mol Ther*. 2021;29(5):1729–1743. https://doi.org/10.1016/j.ymthe.2021.01.020.
16. Ma H, Zhang J, Wu H. Designing Ago2-specific siRNA/shRNA to avoid competition with endogenous miRNAs. *Mol Ther Nucleic Acids*. 2014;3(7), e176. https://doi.org/10.1038/mtna.2014.27.
17. Shang R, Zhang F, Xu B, et al. Ribozyme-enhanced single-stranded Ago2-processed interfering RNA triggers efficient gene silencing with fewer off-target effects. *Nat Commun*. 2015;6:8430. https://doi.org/10.1038/ncomms9430.
18. Martin Perez C, Liang X, Gupta D, et al. *An Extracellular Vesicle Delivery Platform Based on the PTTG1IP Protein*. 4. Extracell Vesicle; 2024. https://doi.org/10.1016/j.vesic.2024.100054.
19. DePolo NJ, Reed JD, Sheridan PL, et al. VSV-G pseudotyped lentiviral vector particles produced in human cells are inactivated by human serum. *Mol Ther*. 2000;2(3):218–222. https://doi.org/10.1006/mthe.2000.0116.
20. Hu S, Mohan Kumar D, Sax C, Schuler C, Akkina R. Pseudotyping of lentiviral vector with novel vesiculovirus envelope glycoproteins derived from Chandipura and Piry viruses. *Virology*. 2016;488:162–168. https://doi.org/10.1016/j.virol.2015.11.012.
21. Munis AM, Mattiuzzo G, Bentley EM, Collins MK, Eyles JE, Takeuchi Y. Use of heterologous vesiculovirus G proteins circumvents the humoral anti-envelope immunity in lentivector-based in vivo gene delivery. *Mol Ther Nucleic Acids*. 2019;17:126–137. https://doi.org/10.1016/j.omtn.2019.05.010.
22. Hwang BY, Schaffer DV. Engineering a serum-resistant and thermostable vesicular stomatitis virus G glycoprotein for pseudotyping retroviral and lentiviral vectors. *Gene Ther*. 2013;20(8):807–815. https://doi.org/10.1038/gt.2013.1.
23. Segel M, Lash B, Song J, et al. Mammalian retrovirus-like protein PEG10 packages its own mRNA and can be pseudotyped for mRNA delivery. *Science*. 2021;373(6557):882–889. https://doi.org/10.1126/science.abg6155.
24. Strebinger D, Frangieh CJ, Friedrich MJ, Faure G, Macrae RK, Zhang F. Cell type-specific delivery by modular envelope design. *Nat Commun*. 2023;14(1):5141. https://doi.org/10.1038/s41467-023-40788-8.
25. Brown DW, Wee P, Bhandari P, et al. Safe and effective in vivo delivery of DNA and RNA using proteolipid vehicles. *Cell*. 2024;187(19):5357–5375 e5324. https://doi.org/10.1016/j.cell.2024.07.023.
26. Hindi SM, Petrany MJ, Greenfeld E, et al. Enveloped viruses pseudotyped with mammalian myogenic cell fusogens target skeletal muscle for gene delivery. *Cell*. 2023;186(10):2062–2077 e2017. https://doi.org/10.1016/j.cell.2023.03.033.
27. Liang X, Gupta D, Xie J, et al. Engineering of extracellular vesicles for efficient intracellular delivery of multimodal therapeutics including genome editors. *Nat Commun*. 2025;16(1):4028. https://doi.org/10.1038/s41467-025-59377-y.
28. Chen S, Saeed A, Liu Q, et al. Macrophages in immunoregulation and therapeutics. *Signal Transduct Targeted Ther*. 2023;8(1):207. https://doi.org/10.1038/s41392-023-01452-1.
29. Gordon S, Martinez FO. Alternative activation of macrophages: mechanism and functions. *Immunity*. 2010;32(5):593–604. https://doi.org/10.1016/j.immuni.2010.05.007.
30. Murray PJ. Macrophage polarization. *Annu Rev Physiol*. 2017;79:541–566. https://doi.org/10.1146/annurev-physiol-022516-034339.
31. Zheng Y, Wang S, Zhong Y, Huang C, Wu X. A20 affects macrophage polarization through the NLRP3 inflammasome signaling pathway and promotes breast cancer progression. *Exp Ther Med*. 2023;25(4):147. https://doi.org/10.3892/etm.2023.11846.
32. Lu M, Xing H, Xun Z, et al. Exosome-based small RNA delivery: progress and prospects. *Asian J Pharm Sci*. 2018;13(1):1–11. https://doi.org/10.1016/j.ajps.2017.07.008.
33. Maheshwari R, Tekade M, Gondaliya P, Kalia K, D'Emanuele A, Tekade RK. Recent advances in exosome-based nanovehicles as RNA interference therapeutic carriers. *Nanomedicine*. 2017;12(21):2653–2675. https://doi.org/10.2217/nnm-2017-0210.
34. Shahabipour F, Barati N, Johnston TP, Derosa G, Maffioli P, Sahebkar A. Exosomes: nanoparticulate tools for RNA interference and drug delivery. *J Cell Physiol*. 2017;232(7):1660–1668. https://doi.org/10.1002/jcp.25766.
35. Rannikko JH, Hollmen M. Clinical landscape of macrophage-reprogramming cancer immunotherapies. *Br J Cancer*. 2024;131(4):627–640. https://doi.org/10.1038/s41416-024-02715-6.
36. Kamerkar S, Leng C, Burenkova O, et al. Exosome-mediated genetic reprogramming of tumor-associated macrophages by exoASO-STAT6 leads to potent monotherapy antitumor activity. *Sci Adv*. 2022;8(7), eabj7002. https://doi.org/10.1126/sciadv.abj7002.
37. Cinelli MA, Do HT, Miley GP, Silverman RB. Inducible nitric oxide synthase: regulation, structure, and inhibition. *Med Res Rev*. 2020;40(1):158–189. https://doi.org/10.1002/med.21599.
38. Brown CR, Gupta S, Qin J, et al. Investigating the pharmacodynamic durability of GalNAc-siRNA conjugates. *Nucleic Acids Res*. 2020;48(21):11827–11844. https://doi.org/10.1093/nar/gkaa670.
39. Liang Y, Duan L, Lu J, Xia J. Engineering exosomes for targeted drug delivery. *Theranostics*. 2021;11(7):3183–3195. https://doi.org/10.7150/thno.52570.
40. Lu M, Shao W, Xing H, Huang Y. *Extracellular vesicle-based nucleic acid delivery*. 2023;1(2), e20220007. https://doi.org/10.1002/INMD.20220007.
41. Lu M, Zhao X, Xing H, et al. Comparison of exosome-mimicking liposomes with conventional liposomes for intracellular delivery of siRNA. *Int J Pharm*. 2018;550(1-2):100–113. https://doi.org/10.1016/j.ijpharm.2018.08.040.
42. Ziqi Wang HX, Huang Yuanyu, Mei Lu. *Extracellular vesicle-based targeted RNA therapies against cancer*. In: *Extracellular Vesicle*. 6. 2025.